'Designer atoms' for quantum metrology

C. F. Roos[1,2], M. Chwalla[1], K. Kim[1], M. Riebe[1], and R. Blatt[1,2]

[1]*Institut für Experimentalphysik, Universität Innsbruck, Technikerstr. 25, A-6020 Innsbruck, Austria*

[2]*Institut für Quantenoptik und Quanteninformation, Österreichische Akademie der Wissenschaften, Otto-Hittmair-Platz 1, A-6020 Innsbruck, Austria*

Entanglement is recognized as a key resource for quantum computation[1] and quantum cryptography[2]. For quantum metrology, the use of entangled states has been discussed[3–5] and demonstrated[6] as as a means to improve the signal-to-noise ratio. In addition, entangled states have been used in experiments for efficient quantum state detection[7] and for the measurement of scattering lengths[8]. In quantum information processing, manipulation of individual quantum bits allows for the tailored design of specific states that are insensitive to the detrimental influences of an environment[9]. Such decoherence-free subspaces[10] protect quantum information and yield significantly enhanced coherence times[11]. Here, we use a decoherence-free subspace with specifically designed entangled states[12] to demonstrate precision spectroscopy; we obtain the electric quadrupole moment of Ca^+ which is of use for frequency standard applications. We find that entangled states are not only useful for enhancing the signal-to-noise ratio in frequency measurements - a suitably designed pair of atoms also allows clock measurements in the presence of strong technical noise. Our technique makes explicit use of non-locality as an entanglement property and provides an approach for designed quantum

metrology.

Metrology seeks to relate all measurements to a precision determination of frequencies. The most precise measurements today are obtained from measuring atomic transition frequencies by monitoring the phase evolution of a superposition of the pertaining states. This is achieved by applying Ramsey's interferometric technique[13] that can be generalized[5] to (maximally) entangled states: Under free precession, the two-atom state $\Psi = \frac{1}{\sqrt{2}}(|u_1\rangle|u_2\rangle + |v_1\rangle|v_2\rangle)$ evolves into the state $\Psi(\tau) = \frac{1}{\sqrt{2}}(|u_1\rangle|u_2\rangle + \exp(i\lambda_\phi\tau)|v_1\rangle|v_2\rangle)$ where the phase evolution rate $\lambda_\phi = [(E_{u_1} + E_{u_2}) - (E_{v_1} + E_{v_2})]/\hbar$ is proportional to the differences in atomic energies E_{u_k}, E_{v_k} of the involved levels. The real part of the phase factor $e^{i\lambda_\phi\tau}$ is measured by projecting the atoms onto the states $|\pm\rangle_k = \frac{1}{\sqrt{2}}(|u_k\rangle \pm |v_k\rangle)$ and measuring the parity operator $P = \hat{P}_{(++)} + \hat{P}_{(--)} - \hat{P}_{(+-)} - \hat{P}_{(-+)}$, where $\hat{P}_{(\pm,\pm)}$ denotes the projector onto the state $|\pm\rangle_1 \otimes |\pm\rangle_2$. If Ψ belongs to a decoherence-free subspace, free precession times τ of several seconds[14,15] allow for highly accurate phase estimation.

In atomic optical frequency standards based on single hydrogen-like trapped ions[16], the transition frequency from the S ground state to a metastable D_j state is measured by an optical frequency comb[17]. The D_j state's atomic electric quadrupole moment interacting with residual electric quadrupole fields[18] gives rise to frequency shifts of a few Hertz. The shift of the Zeeman sublevel $|D_j, m_j\rangle$ in a quadrupole field $\Phi(x, y, z) = A(x^2 + y^2 - 2z^2)$ is given by

$$\hbar\Delta\nu = \frac{1}{4}\frac{dE_z}{dz}\Theta(D, j)\frac{j(j+1) - 3{m_j}^2}{j(2j-1)}(3\cos^2\beta - 1), \tag{1}$$

where $dE_z/dz = 4A$ is the electric field gradient along the potential's symmetry axis z, β denotes the angle between the quantization axis z and $\Theta(D, j)$ expresses the strength of the quadrupole

moment in terms of a reduced matrix element[18].

Recently, quadrupole moments have been measured for $^{88}Sr^{+}$, $^{199}Hg^{+}$ and $^{171}Yb^{+}$ with a precision ranging from about 4% to 12% (refs. [20–22]). In these single-ion experiments, narrow-linewidth lasers are employed to detect electric quadrupole shifts by measuring the transition frequency from the electronic ground state to the metastable state. Alternatively, the quadrupole shift could also be measured by performing Ramsey experiments with an ion prepared in a superposition of Zeeman D_j sublevels. Both measurement schemes are subject to phase decoherence. Laser frequency noise limits the coherence time if the S state is used as the reference state. Magnetic field noise giving rise to first-order Zeeman shifts renders the measurement scheme based on D state superpositions difficult. However, both sources of phase noise can be eliminated by replacing the single ion by a two-ion entangled state prepared in a decoherence-free subspace. Ramsey experiments with the two-ion Bell state $\Psi = \frac{1}{\sqrt{2}}(|m_1\rangle|m_2\rangle + |m_3\rangle|m_4\rangle)$, where the magnetic quantum numbers m_i of the states $|m_i\rangle \equiv |D_j, m_i\rangle$ satisfy $m_1 + m_2 = m_3 + m_4$, are not affected by fluctuations of the magnetic fields to first order since both parts of the superposition are Zeeman-shifted by the same amount (see Fig. 1b). Also, frequency noise of the laser used for preparing Ψ is relevant only during the comparatively short state preparation and read-out steps but not during the long interrogation period. For suitably chosen values of $m_1, \ldots m_4$, a decoherence-immune state can be designed that is sensitive to the electric quadrupole shift (Fig. 1c).

The isotope $^{40}Ca^{+}$ has a single valence electron and no hyperfine structure (Fig. 1a). For its metastable $3d^2D_{5/2}$ state (lifetime $\tau_{D_{5/2}} = 1.168(7)$ s), a quadrupole moment of $1.917\,\mathrm{ea}_0^2$ was

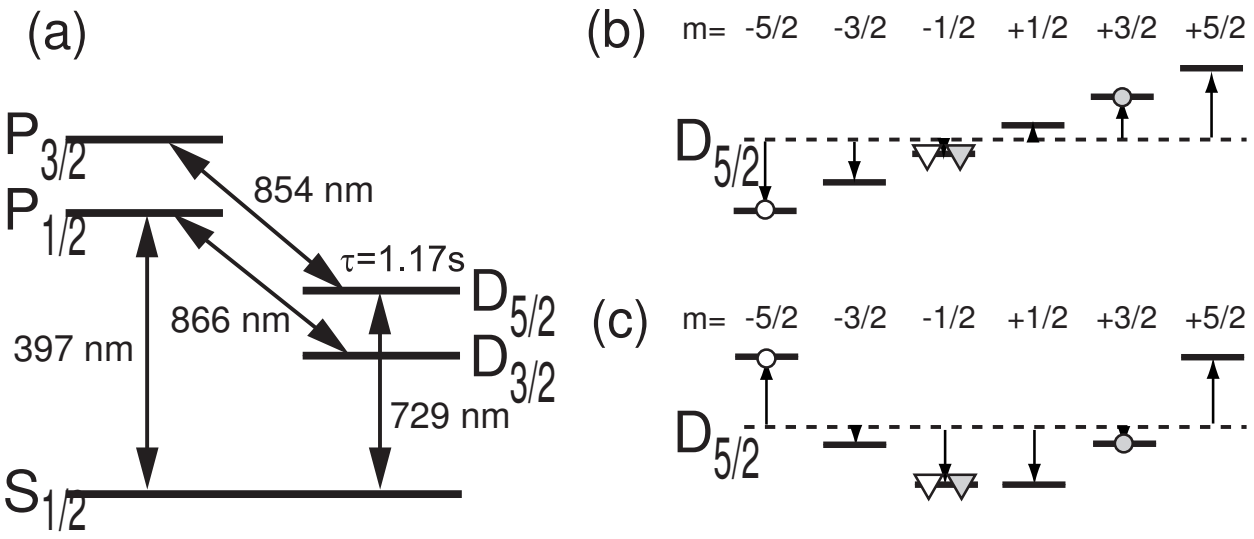

Figure 1: Relevant atomic levels of the $^{40}Ca^{+}$. (a) Bell states are prepared by coherently exciting the $S_{1/2} \leftrightarrow D_{5/2}$ quadrupole transition. The $S_{1/2} \leftrightarrow P_{1/2}$ is used for quantum state read-out, lasers at 866 and 854 serve as repumping and quenching lasers. (b) Energy level shift of the $|m\rangle \equiv |D_{5/2}, m\rangle$ states in a weak magnetic field. (c) Energy level shift caused by an electric quadrupole potential. Energy levels occurring in the state $\Psi_1 = \frac{1}{\sqrt{2}}(|\circ\rangle|\bullet\rangle + |\triangledown\rangle|\blacktriangledown\rangle)$ (eq. (2)) are denoted by the symbols $\circ, \triangledown, \bullet, \blacktriangledown$, the open (filled) symbols corresponding to levels occupied by atom 1 (2), respectively. The combined Zeeman energy of the $|\circ\rangle|\bullet\rangle$-states equals the energy of the $|\triangledown\rangle|\blacktriangledown\rangle$-states, making Ψ_1 immune against magnetic field noise. Since an electric quadrupole field shifts the $|\circ\rangle|\bullet\rangle$- and $|\triangledown\rangle|\blacktriangledown\rangle$-states in opposite directions, Ψ_1 is suitable for a measurement of the quadrupole shift.

calculated[19]. For the experiment, two $^{40}Ca^{+}$ ions are trapped along the axis of a linear ion trap. By applying a static (dc) voltage ranging from 500 to 2000 V to the tip electrodes[23], axial center-of-mass (COM) mode trap frequencies ω_z ranging from 850 to 1700 kHz are achieved, leading to distances between the ions from $6.2\,\mu m$ to $3.9\,\mu m$. A CCD camera images the ions' fluorescence. The degeneracy of the Zeeman states is lifted by applying a magnetic bias field of 2.9 G. The ions are cooled to the ground state of the axial COM mode by Doppler and sideband cooling[24]. For coherent quantum state manipulation, the ions are individually excited on the $|S\rangle \equiv S_{1/2}(m = -1/2) \leftrightarrow |D\rangle \equiv D_{5/2}(m = -1/2)$ transition by a tightly focussed laser beam (laser linewidth ≈ 150 Hz) resonant with either the carrier transition or the upper motional sideband. For a detailed description of the experimental setup, see ref.[23].

The Bell state $\Psi_{SD}^{\pm} = (|S\rangle|D\rangle \pm |D\rangle|S\rangle)/\sqrt{2}$ is created with a fidelity of about 90% by a sequence of three laser pulses[11]. Additional carrier π pulses transfer the entanglement into the $D_{5/2}$ Zeeman state manifold, thus generating the state

$$\Psi_1 = \frac{1}{\sqrt{2}}(|-5/2\rangle|+3/2\rangle + |-1/2\rangle|-1/2\rangle). \tag{2}$$

This magnetic field-insensitive state is used for a measurement of the quadrupole shift. In the vicinity of the trap center, the dc voltage applied to the tip electrodes creates a rotationally symmetric electric quadrupole potential which shifts the energy of the constituents of the superposition state Ψ_1 by $\hbar\Delta_1 = 24/5\,\hbar\delta$ with respect to each other. Here, $\hbar\delta$ is the shift that a single ion in state $|-5/2\rangle$ would experience. The two-ion shift is bigger by $12/5$ because two ions contribute that are prepared in substates which shift in opposite directions. In addition, the presence of a second ion doubles the electric field gradient at the location of the other ion[12]. For the shift measurement,

Ψ_1 is let to evolve into $\Psi_1(\tau) = \frac{1}{\sqrt{2}}(|-5/2\rangle|+3/2\rangle + \exp(i\Delta_1\tau)|-1/2\rangle|-1/2\rangle)$ and $\cos(\Delta_1\tau)$ is measured for τ ranging from 0 to 300 ms. Figure 2a shows the resulting parity oscillations[11] at a frequency $\Delta_1 = (2\pi)\,33.35(3)$ Hz. Disentanglement of $\Psi_1(\tau)$ by spontaneous decay manifests itself as damping of the oscillations with a damping time constant $\tau_d = 587(70)$ ms close to the expected value $\frac{1}{2}\tau_{D_{5/2}} = 584$ ms. Parity oscillations of the state $\Psi_2(\tau) = \frac{1}{\sqrt{2}}(|3/2\rangle|-5/2\rangle + \exp(i\Delta_2\tau)|-1/2\rangle|-1/2\rangle)$ are shown in Fig. 2b. Its oscillation frequency $\Delta_2 = (2\pi)\,36.52(4)$ Hz slightly differs from Δ_1 because of a magnetic field gradient in the direction of the ion crystal that gives rise to an additional contribution to the parity signal[12]. Both phase oscillation contributions can be separately determined by taking the average $\Delta = (\Delta_1 + \Delta_2)/2$ and the difference $\Delta_{B'} = |\Delta_1 - \Delta_2|/2$ of the signals. By recording parity oscillations at different tip voltages U_{tips}, we measure the quadrupole shift $\Delta/(2\pi)$ as function of the electric field gradient and observe a linear change in $\Delta(U_{tips})$.

For a precise determination of the quadrupole moment, the dependence of the quadrupole shift on the orientation of the magnetic field should be minimized. We investigate the angle dependence of Δ by varying the orientation of the magnetic field in a plane that also contains the z-axis of the trap. Initialization of the ions in a pure state prior to coherent manipulation is achieved by optical pumping on the quadrupole transition (see Methods). Generally, it cannot be excluded that the quadrupole field has imperfect rotational symmetry. In this case, the factor $3\cos^2(\beta) - 1$ in eq.(1) needs to be replaced by $(3\cos^2\beta - 1) - \epsilon\sin^2\beta\cos(2\alpha)$ where ϵ characterizes the asymmetry and α its direction[18]. Note, however, that the additional term vanishes for $\beta = 0$. Figure 3 shows the sinusoidal variation of Δ measured at $U_{tips} = 1000$ V as a function of the angle. At

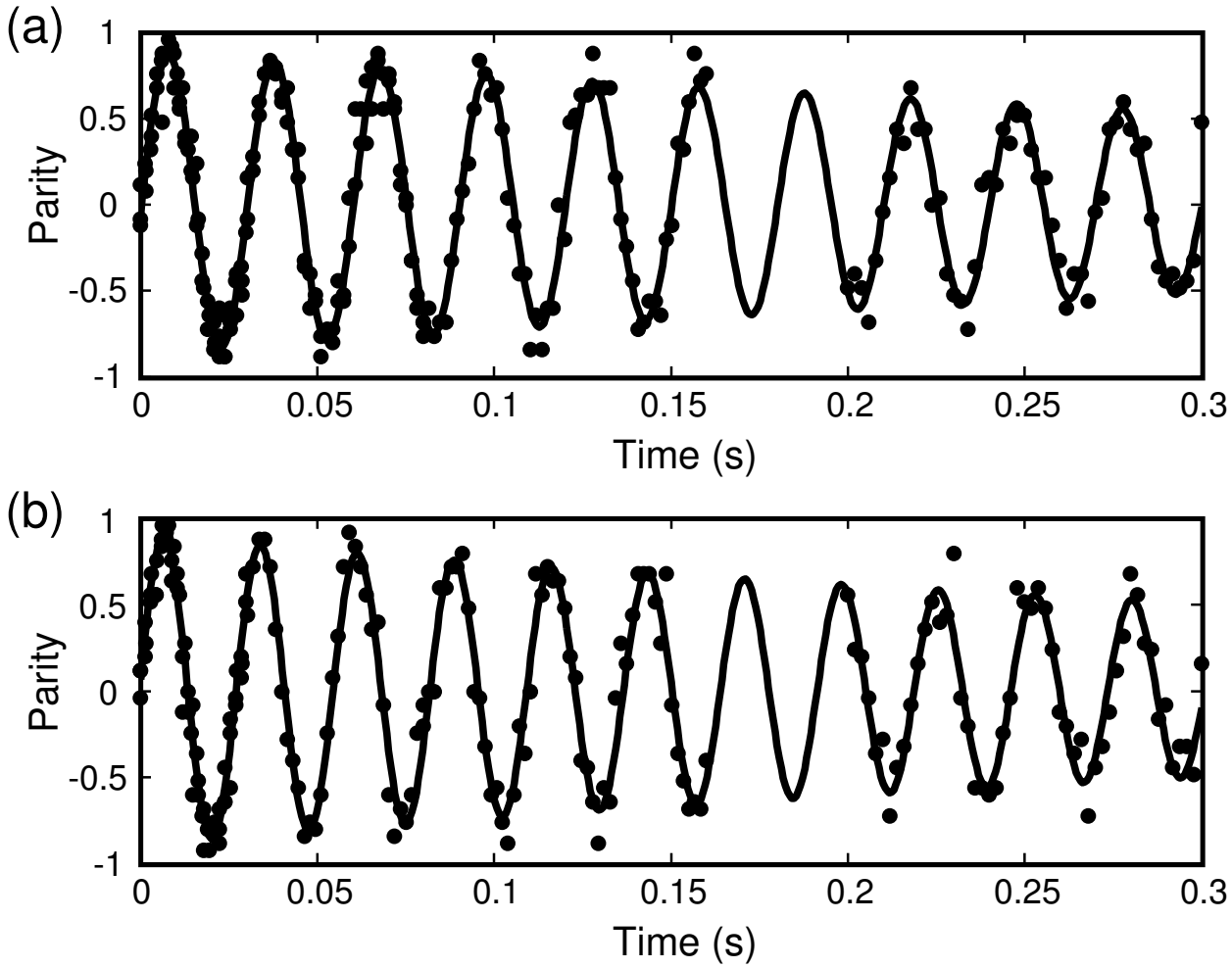

Figure 2: Parity oscillations of the entangled states Ψ_1 and Ψ_2 at $U_{tips} = 750$ V tip voltage. The experiment is repeated 100 times for each data point. An exponentially damped sinusoidal function is fitted to the data. (a) For Ψ_1, the oscillation frequency is $\Delta_1 = (2\pi)\, 33.35(3)$ Hz and the damping time $587(70)$ ms. (b) For Ψ_2, the fit yields $\Delta_2 = (2\pi)\, 36.52(4)$ Hz and a decay time $525(60)$ ms. For each plot, five different datasets were merged. No data were taken covering waiting times around 170 ms. To exclude slow drifts of the initial parity over time, data for waiting times up to 20 ms were repeatedly taken.

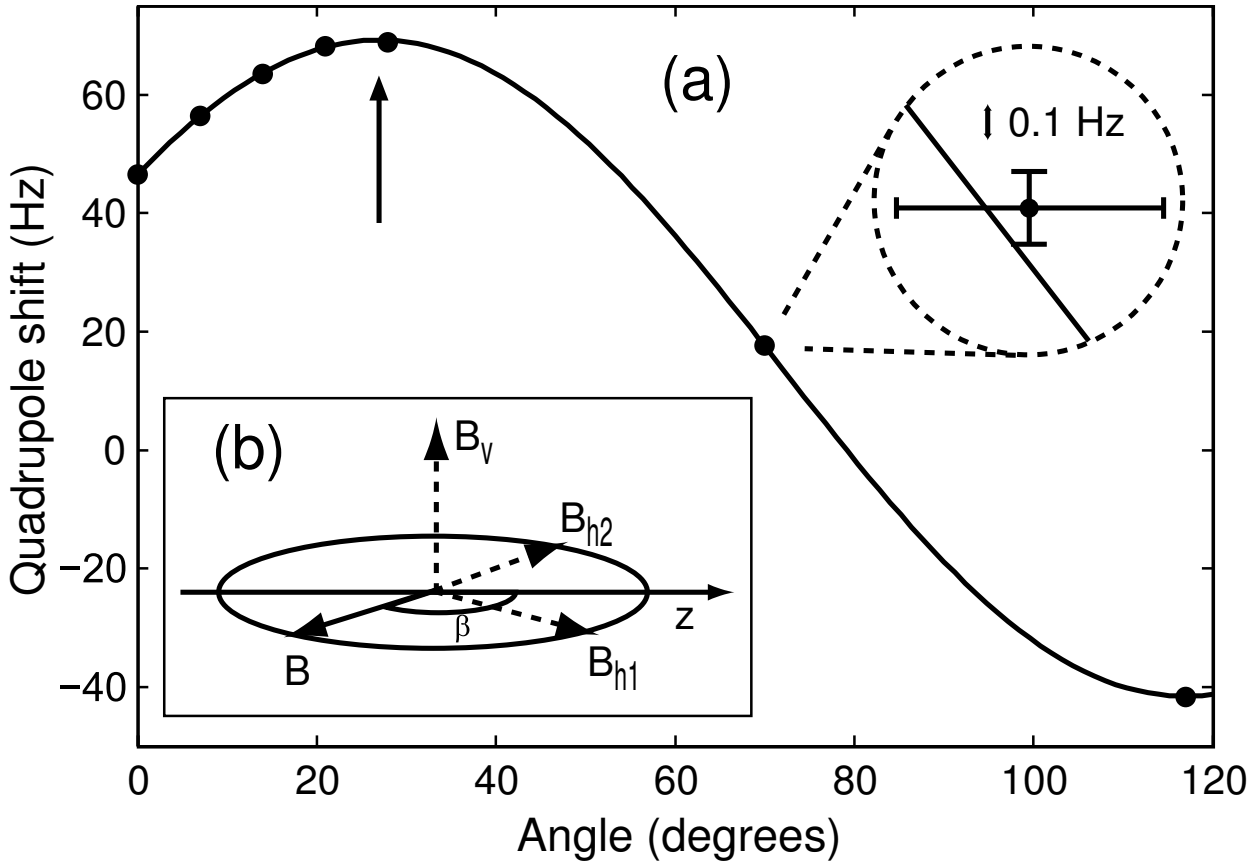

Figure 3: (a) Quadrupole shift $\Delta/(2\pi)$ at $U_{tips} = 1000$ V as a function of the magnetic field orientation $\beta - \beta_0$. The data are fitted by $\Delta = \Delta_a + \Delta_b \cos^2(\beta - \beta_0)$, yielding $\beta_0 = 26.9°$. The arrow indicates the angle corresponding to $\beta = 0$. For the determination of the quadrupole moment, shift measurements are performed at $\beta = 0$ since errors in β enter the calculation only in second order. Note that the error bars are smaller than the point size. The inset in the upper right corner shows an enlarged data point. (b) Geometry of magnetic field coils. The angle β is varied by appropriately changing the current in pairs of coils producing the magnetic fields B_{h1}, B_{h2}. Field B_v is used to null residual fields in the perpendicular direction.

the angle that maximizes Δ, another maximization is performed in the perpendicular direction to determine the direction corresponding to $\beta = 0$. Figure 4a displays the quadrupole shift measured at $\beta = 0$ as a function of the electric field gradient dE_z/dz. Using $dE_z/dz = -m\omega_z^2/e$, the gradient is calibrated by a measurement of the ion's oscillation frequency ω_z. By fitting a straight line $\Delta/(2\pi) = \Delta_0/(2\pi) + a\frac{dE_z}{dz}$ to the data, we determine the slope $a = 2.975(2)$ Hz mm^2/V and the offset $\Delta_0/(2\pi) = -2.4(1)$ Hz. The major part of the phase oscillation frequency Δ_0 at $\frac{dE_z}{dz} = 0$ is caused by the second-order Zeeman effect that contributes $\Delta_{B^2}/(2\pi) = -2.9$ Hz at the bias field of 2.9 G. The remaining part $\Delta_0 - \Delta_{B^2}$ is attributed to a residual quadrupole field caused by stray charges. The quadrupole moment $\Theta(3d, 5/2) = \frac{5}{12}ha$ is proportional to the slope a. While the uncertainty in the value of a is smaller than 10^{-3}, the main uncertainty in $\Theta(3d, 5/2)$ is due to errors in the determination of the angle β. Assuming that the angle can be determined with an accuracy of 3 degrees (see Methods), we determine the quadrupole moment to be $\Theta(3d, 5/2) = 1.83(1)\mathrm{ea}_0^2$.

These results show the viability of the approach of designing specific entangled states for precision measurements. For frequency standard applications, minimization of the quadrupole shift is imperative[25,26]. Note that, by using the designed entangled states $|S_{1/2}, m=1/2\rangle|S_{1/2}, m=-1/2\rangle + |D_{5/2}, m'\rangle|D_{5/2}, -m'\rangle$, the quadrupole could be cancelled by averaging the results over states with $m' \in \{\frac{1}{2}, \frac{3}{2}, \frac{5}{2}\}$. The design approach demonstrated here is new to metrology: whereas previously the use of entangled states was to enhance the signal-tonoise ratio, the use of a designed pair of entangled ions allows an atomic clock measurement to be performed in a subspace free of magnetic field noise. This is achieved with unprecedented precision on an even isotope, which Q8 opens the way to optical frequency standards based on a whole variety of easily accessible atomic

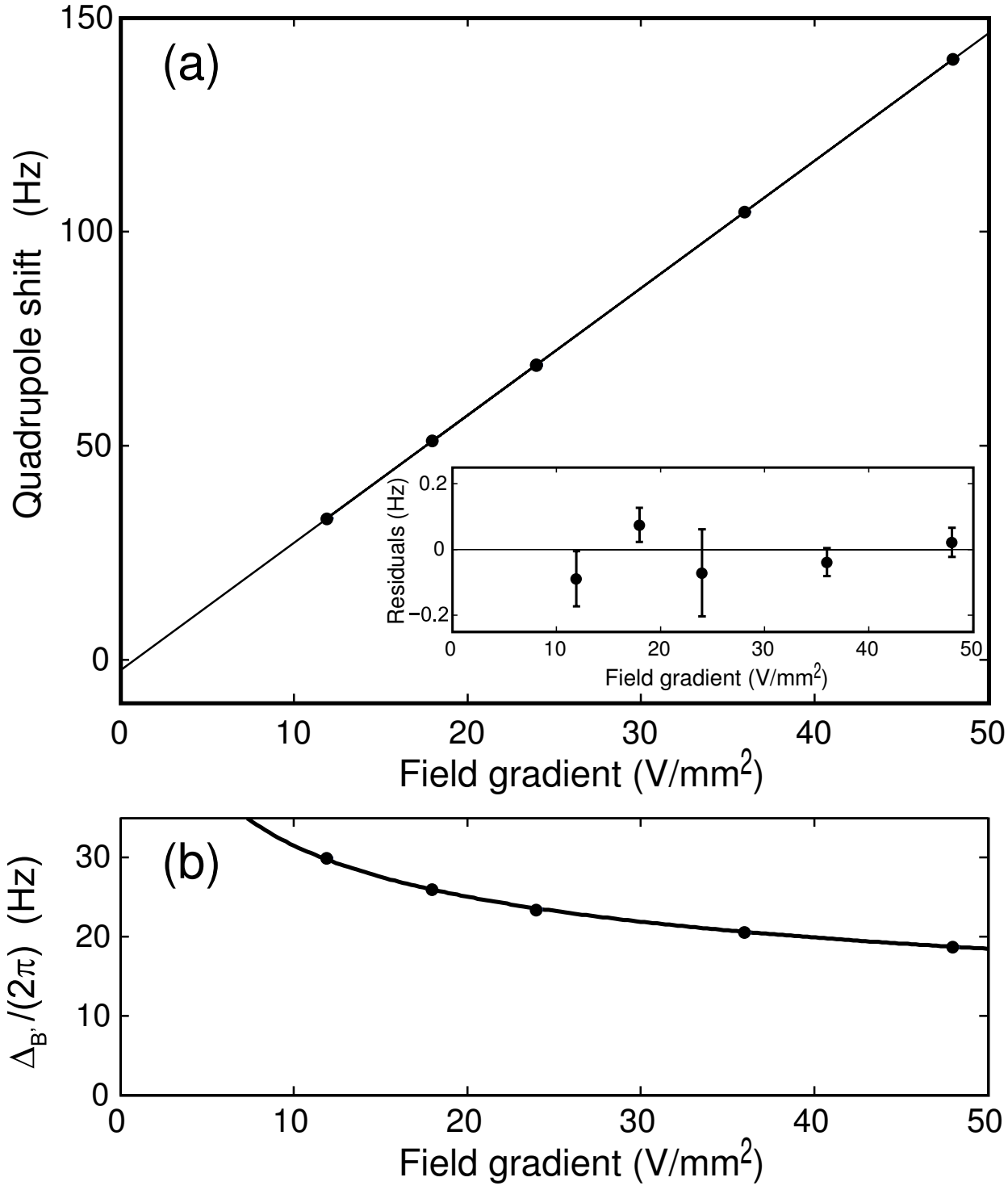

Figure 4: (a) Quadrupole shift as a function of the applied external electric field gradient dE_z/dz. The offset at $dE_z/dz = 0$ is mainly due to the second-order Zeeman effect. The quadrupole moment is proportional to the slope which is measured with an uncertainty of less than 0.1%. The inset shows the deviation of the data points from the linear fit. (b) Phase oscillation rate $\Delta_{B'}/(2\pi)$ due to the magnetic field gradient calculated from $|\Delta_2 - \Delta_1|/2$. Since the distance d between the ions decreases at higher electric field gradients, $\Delta_{B'} \propto d \propto (dE_z/dz)^{-1/3}$.

systems not considered so far.

Methods

Frequency-resolved optical pumping. Due to the magnetic bias field, the ions can be prepared in the $|S_{1/2}, m = -1/2\rangle$ state for an arbitrary orientation of the magnetic field by frequency-resolved optical pumping on the quadrupole transition. For this, the $|S_{1/2}, m = +1/2\rangle \leftrightarrow |D_{5/2}, m = -3/2\rangle$ transition is excited while the repumping lasers on the $D_{5/2} \leftrightarrow P_{3/2}$ and $D_{3/2} \leftrightarrow P_{1/2}$ transitions are switched on at the same time. After an excitation of 1 ms duration, at least 99.9% of the population has been pumped to the $|S_{1/2}, m = -1/2\rangle$ state.

Orientation of the magnetic field. The magnetic field $\vec{B}$ is set by passing currents I_{h_1}, I_{h_2}, I_v through three mutually orthogonal pairs of coils (see Fig. 3 b). We calibrate the field coils and null the offset currents by measuring the Zeeman shift of the $|S_{1/2}, m = -1/2\rangle \leftrightarrow |D_{5/2}, m = -1/2\rangle$ transition as a function of the currents. After nulling the field in the v-direction, we map out the values of (I_{h_1}, I_{h_2}) that yield a constant Zeeman shift and fit an ellipse to the data. These current values rotate $\vec{B}$ in a horizontal plane that also contains the symmetry axis (z) of the ion trap. A similar procedure is applied for calibrating the v-coil.

Alignment of the magnetic field with the trap axis. A residual quadrupole potential Φ_s caused by stray charges and by voltages applied to the compensation electrodes will lead to errors in the alignment of the magnetic field $\vec{B}$ with the principal axis of the trap's electric quadrupole potential Φ_{tips}. This is due to the fact that $\vec{B}$ is aligned with the direction $\vec{n}_{ts}$ that maximizes the quadrupole

shift of $\Phi_{tips}(\vec{n}) + \Phi_s(\vec{n})$ instead of the direction $\vec{n}_t$ that would be chosen without Φ_s. Fortunately, Φ_s is much smaller than Φ_{tips} in the experiment. We obtain information about the magnitude of Φ_s by (1) extrapolating the ion oscillation frequency $\omega_z(U_{tips})$ for $U_{tips} \rightarrow 0$, (2) measuring the electric stray field $\vec{E}_s$ and assuming the magnitude of the field gradient to be $\propto |E_s|/r$ where r is the smallest distance of the ions from the trap electrodes. Most importantly, (3) by measuring the residual quadrupole shifts for $\beta = 0$ and another direction with $\beta = 26.9°$, constraints regarding the shape, orientation and magnitude of Φ_s can be found that allow us to calculate the average angle $\Delta\beta$ between $\vec{n}_{ts}$ and $\vec{n}_t$. We find $\Delta\beta = 3°$ and use this value for estimating the uncertainty in the determination of $\Theta(3d, 5/2)$.

1. M. A. Nielsen, I. L. Chuang, *Quantum computation and quantum information*, (Cambridge Univ. Press, Cambridge, 2000).

2. N. Gisin, G. Ribordy, W. Tittel, and H. Zbinden, Quantum cryptography, *Rev. Mod. Phys.* **74**, 145–195 (2002).

3. V. Giovannetti, S. Loyd, and L. Maccone, Quantum-enhanced measurements: beating the standard quantum limit, *Science* **306**, 1330–1336 (2004).

4. V. Giovannetti, S. Loyd, and L. Maccone, Quantum metrology, *Phys. Rev. Lett.* **96**, 010401 (2006).

5. J. J. Bollinger, W. M. Itano, D. J. Wineland, and D. J. Heinzen, Optimal frequency measurements with maximally correlated states, *Phys. Rev. A* **54**, R4649–4652 (1996).

6. D. Leibfried *et al.*, Toward Heisenberg-limited spectroscopy with multiparticle entangled states, *Science* **304**, 1476–1478 (2004).

7. P. O. Schmidt, T. Rosenband, C. Langer, W. M. Itano, J. C. Bergquist, and D. J. Wineland, Spectroscopy using quantum logic, *Science* **309**, 749–752 (2005).

8. A. Widera *et al.*, Entanglement interferometry for precision measurement of atomic scattering properties, *Phys. Rev. Lett.* **92**, 160406 (2004).

9. D. Kielpinski *et al.*, A decoherence-free quantum memory using trapped ions, *Science* **291**, 1013–1015 (2001).

10. D. A. Lidar, I. L. Chuang, and K. B. Whaley, Decoherence-free subspaces for quantum computation, *Phys. Rev. Lett.* **81**, 2594 (1998).

11. C. F. Roos *et al.*, Bell states with ultra-long lifetimes and their tomographic state analysis, *Phys. Rev. Lett.* **92**, 220402 (2004).

12. C. F. Roos, Precision frequency measurements with entangled states, *arXiv*:quant-ph/0508148 (2005).

13. N. F. Ramsey, A molecular beam resonance method with separated oscillating fields, *Phys. Rev.* **78**, 695–699 (1950).

14. H. Häffner *et al.*, Robust entanglement, *Appl. Phys. B* **81**, 151–153 (2005).

15. C. Langer *et al.*, Long-lived qubit memory using atomic ions, *Phys. Rev. Lett.* **95**, 060502 (2005).

16. A. A. Madej, and J. E. Bernard, Single-ion optical frequency standards, in *Frequency measurement and control*, Topics. Appl. Phys. **79**, 153–195 (2001).

17. S. A. Diddams, J. C. Bergquist, S. R. Jefferts, and C. W. Oates, Standards of time and frequency at the outset of the 21st century. *Science*, **306**, 1318–1324 (2004).

18. W. M. Itano, External-field shifts of the $^{199}Hg^{+}$ optical frequency standard, *J. Res. Natl. Inst. Stand. Technol.* **105**, 829–837 (2000).

19. W. M. Itano, Quadrupole moments and hyperfine constants of metastable states of Ca^{+}, Sr^{+}, Ba^{+}, Yb^{+}, Hg^{+}, and Au, *Phys. Rev. A* **73**, 022510 (2006).

20. W. H. Oskay, W. M. Itano, and J. C. Bergquist, Measurement of the $^{199}Hg^{+}$ $5d^{9}6s^{2}\ ^{2}D_{5/2}$ electric quadrupole moment and a constraint on the quadrupole shift, *Phys. Rev. Lett.* **94**, 163001 (2005).

21. G. P. Barwood, H. S. Margolis, G. Huang, P. Gill, and H. A. Klein, Measurement of the electric quadrupole moment of the 4d $^{2}D_{5/2}$ level in $^{88}Sr^{+}$, *Phys. Rev. Lett.* **93**, 133001 (2004).

22. T. Schneider, E. Peik, and Chr. Tamm, Sub-Hertz optical frequency comparisons between two trapped $^{171}Yb^{+}$ ions, *Phys. Rev. Lett.* **94**, 230801 (2005).

23. F. Schmidt-Kaler *et al.*, How to realize a universal quantum gate with trapped ions, *Appl. Phys. B* **77**, 789-796 (2003).

24. Ch. Roos *et al.*, Quantum state engineering on an optical transition and decoherence in a Paul trap, *Phys. Rev. Lett.* **83**, 4713–4716 (1999).

25. H. S. Margolis *et al.* Hertz-level measurement of the optical clock frequency in a single $^{88}Sr^{+}$ ion, *Science* **306**, 1355–1358 (2004).

26. P. Dubé *et al.*, Electric quadrupole shift cancellation in single-ion optical frequency standards, *Phys. Rev. Lett.* **95**, 033001 (2005).

Acknowledgements We thank H. Häffner for his contributions to the optical pumping scheme. We gratefully acknowledge support by the Austrian Science Fund (FWF), by the European Commission (SCALA, CONQUEST networks), and by the Institut für Quanteninformation GmbH. This material is based upon work supported in part by the U. S. Army Research Office.

Competing Interests The authors declare that they have no competing financial interests.

Correspondence Correspondence and requests for materials should be addressed to C.R.

(email: christian.roos@uibk.ac.at).